Characterization of the Electrochemical Oxidation of Peroxynitrite: Relevance to Oxidative Stress Bursts Measured at the Single Cell Level

Christian Amatore,*[a] Stéphane Arbault,[a] Delphine Bruce,[a] Pedro de Oliveira,[a] Marie Erard,[a] and Monique Vuillaume[a, b]

Abstract: The electrochemical signature of peroxynitrite oxidation is reported for the first time, and its mechanism discussed in the light of data obtained by steady-state and transient voltammetry at microelectrodes. Peroxynitrite is an important biological species generated by aerobic cells presumably via the near diffusion-limited coupling of nitric oxide and superoxide ion. Its production by living cells has been previously suspected during cellular oxidative bursts as well as in several human pathologies (arthritis, inflammation, apoptosis, ageing, carcinogenesis, Alzheimer disease, AIDS, etc.). However, this could only be inferred on the basis of characteristic patient metabolites or through indirect detection, or by observation of follow-up species resulting supposedly from its chemical reactions in vivo. In this work, thanks to the independent knowledge of the electrochemical characteristics of ONO_2^- oxidation, the kinetics and intensity of this species released by single human fibroblasts could be established directly and quantitatively based on the application of the artificial synapse method. It was then observed and established that fibroblasts submitted to mechanical stresses produce oxidative bursts, which involve the release within less than a tenth of a second of a complex cocktail composed of several femtomoles of peroxynitrite, hydrogen peroxide, nitric oxide, and nitrite ions.

Keywords: electrochemistry · microelectrodes · oxidative stress · peroxynitrite · voltammetry

Introduction

Aerobic cells actively produce reactive oxygen and nitrogen species when their integrity is threatened by environmental hazards such as infectious entities (e.g. viruses, bacteria), xenobiotics (e.g. water and air pollutants), and physical agents (e.g. high-energy radiation, UV light, mechanical intrusion). Such an increase in oxidizing species is generally compensated for by reducing substances (vitamins, glutathion, catalase, superoxide dismutase (SOD), and so on). When this delicate balance is upset, a metabolic condition known as oxidative stress prevails.[1–3]

This situation is supposed to originate from an increased production of superoxide ion ($O_2^{\bullet -}$) and nitrogen monoxide ($NO^{\bullet}$) by cells. Superoxide is constantly generated by aerobic cells as an unwanted side product (6–8% of metabolic oxygen) during their normal metabolism.[1, 4–6] Under oxidative stress conditions, much more significant quantities of $O_2^{\bullet -}$ may be produced through the involvement of NADPH-oxidase type enzymes [Eq. (1)].[7–9]

$$2\,O_2 + NADPH \longrightarrow 2\,O_2^{\bullet -} + NADP^+ + H^+ \quad (1)$$

Under normal conditions, most of this hazardous species is readily scavenged through its fast disproportionation into hydrogen peroxide and oxygen [Eqs. (2)–(4)].

$$O_2^{\bullet -} + H^+ \rightleftharpoons HOO^{\bullet} \ (K_{pH=7} \ll 1) \quad (2)$$

$$HOO^{\bullet} + O_2^{\bullet -} \longrightarrow HOO^- + O_2 \ (\text{fast}) \quad (3)$$

$$HOO^- + H^+ \longrightarrow H_2O_2 \ (\text{fast}) \quad (4)$$

In living aerobic cells, this fast process is even accelerated by its catalysis by superoxide dismutase (SOD, rate constant: $k_{SOD} = 2.5 \times 10^9\,M^{-1}s^{-1}$ at pH = 7) [Eq. (5)].[10]

$$2\,O_2^{\bullet -}\ (+\,2H^+)_{pH=7} \longrightarrow H_2O_2 + O_2 \quad (5)$$

The release of $NO^{\bullet}$ is thought to originate from the activation of cell NO-synthases [Eq. (6)].[11, 12]

$$\text{L-arginine} + 2\,NADPH + 2\,O_2 + 2\,H^+ \longrightarrow NO^{\bullet} + \text{citrulline} + 2\,NADP^+ + 2\,H_2O \quad (6)$$

[a] Prof. C. Amatore, Dr. S. Arbault, Dr. D. Bruce, Dr. P. de Oliveira M. Erard, Dr. M. Vuillaume
Ecole Normale Supérieure, Département de Chimie
UMR CNRS 8640 PASTEUR
24 rue Lhomond, 75231 Paris cedex 05 (France)
Fax: (+33) 1-4432-3863
E-mail: amatore@ens.fr

[b] Dr. M. Vuillaume
Institut A. Lwoff, UPR CNRS 2169, 7 rue G. Moquet
BP 8, 94801 Villejuif (France)

  0947-6539/01/0719-4171 $ 17.50+.50/0

Moreover, $O_2^{\bullet-}$ and $NO^{\bullet}$ couple at a rate constant close to the diffusion limit ($\approx 2 \times 10^{10}\,M^{-1}s^{-1}$)[13] to form peroxynitrite ion, ONO_2^- [Eq. (7)].

$$NO^{\bullet} + O_2^{\bullet-} \longrightarrow ONO_2^- \quad (7)$$

Peroxynitrite is a short-lived species under physiological conditions ($t_{1/2} \approx 1$ s at $T = 25\,^{\circ}C$ for pH = 7.4) since it decomposes via the intermediate formation of its conjugated acid ONO_2H ($pK_a = 6.8$) into nitrate and nitrite ions.[13] However, it displays a wide range of biochemical reactivity since it has been shown:

1) to nitrate proteins (tyrosine residues), carbohydrates, and nucleic acids;
2) to oxidize lipids, thiol groups, Fe/S and Zn/S centers,[14] and oxyhemoglobin to methemoglobin;
3) to freely cross the cytoplasmic membrane of red blood cells when protonated.[15]

Also, it readily reacts with CO_2 to form nitrosoperoxycarbonate, $ONO_2CO_2^-$, which is supposed to be a very efficient nitrating species[16, 17] although it rapidly decays to CO_2 and NO_3^-. As a consequence, peroxynitrite has been associated with several pathological conditions such as arthritis, inflammation, apoptosis, ageing, carcinogenesis, strokes, Alzheimer's, Huntington and Parkinson's diseases, AIDS, and acute ischemia-reperfusion injury.[18–21]

So far, the involvement of ONO_2^- in these oxidative stress processes has been only indirectly inferred from patients' metabolites and by detecting species supposedly resulting from its chemical action: free radicals studied by chemiluminescence;[22] increase of the methemoglobin/oxyhemoglobin ratio as measured by spectrophotometry;[23, 24] presence of nitrated amino acids as detected spectrophotometrically and by Western blot analysis.[23] An indirect amperometric detection method based on the reduction of ONO_2^- by using a redox mediator has also been recently described[25] but, to the best of our knowledge, no data have ever been reported on the direct electrochemical oxidation of ONO_2^-.

Here, we present a real-time, electrochemical investigation of ONO_2^- production and release during an oxidative burst at the level of a human cell (fibroblast). This work is based on the use of an artificial synapse method (Figure 1).[26] One half of the synapse is composed of a single living cell, which is stimulated by the fast pricking of its membrane with a sealed micropipette (1 μm radius) to elicit the oxidative burst by mechanical stimulation. A platinized carbon microelectrode placed 5 μm above the puncture hole constitutes the other half of the synapse. The extremely minute release of chemicals that occurs within the artificial cleft after the cell stimulation may then be analyzed in real time with subfemtomole, subsecond resolution.[27, 28]

Recent results obtained by this method have shown the complexity of the cellular burst response.[29, 30] This is composed of several species resulting from the initial production of $NO^{\bullet}$ and $O_2^{\bullet-}$. The results presented below for the oxidative burst reveal the presence of at least three different electrochemical waves, which were compared with the known oxidation waves of the species thought to be involved in the response, namely H_2O_2, $NO^{\bullet}$, and NO_2^-. The short response time of our setup (≈ 0.1 s) allowed us to consider the involvement of unstable species like peroxynitrite. However, before assigning ONO_2^- to one of these waves, its electrochemical signature had first to be obtained. This was investigated at the same platinized carbon fiber disks that were used in our cell experiments. Yet, at high scan rates, when capacitive currents would have altered the voltammetric information at these dendritic electrodes, regular platinum disk microelectrodes were used instead. The chemical fate of the $ONO_2^{\bullet}$ radical generated after the one-electron oxidation of peroxynitrite is discussed on the basis of the electrochemical results.

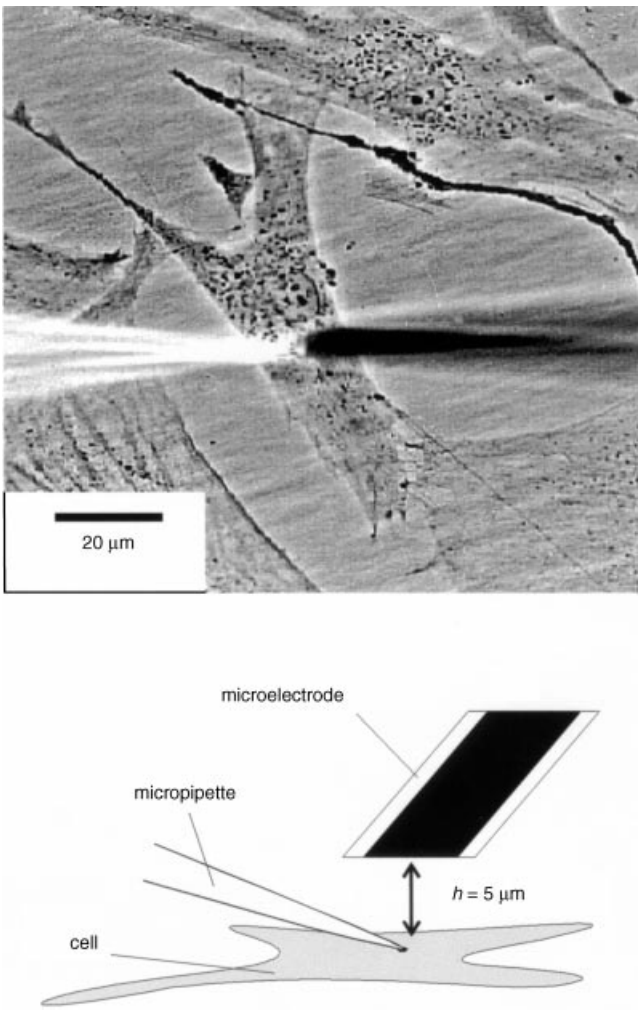

Figure 1. Optical microscopic view and schematic side view showing a human fibroblast in a Petri dish and the positioning of a microelectrode (black shadow on right) which constitute together a semiartificial synapse. A glass micropipette (white shadow on left) used to trigger the oxidative stress response is also seen. The microelectrode and the micropipette appear as shadows on the optical microscopic view because they are out of focus and are located above the cell plane (see scheme).

Results and Discussion

Electrochemical monitoring of superoxide and nitric oxide derivatives at the single cell level: Oxidative stresses induced in human fibroblasts (used as models of skin carcinogenesis in our studies)[31] may be investigated electrochemically through

0947-6539/01/0719-4172 $ 17.50+.50/0 *Chem. Eur. J.* **2001**, *7*, No. 19

the artificial synapse method described above (Figure 1). The electrodes consisted of carbon disks of approximately 10 μm diameter obtained from the cross section of a carbon fiber sealed into a thin soft glass case.[32] The exposed carbon disk was beveled, polished, and platinized so as to increase its electrochemical activity towards small oxygen-containing molecules expected to be released in oxidative bursts (vide supra). The electrode was placed in the desired position above an isolated living cell with a micromanipulator under optical microscopy control (Figure 1).[26]

Oxidative bursts were stimulated by the fast pricking of the cell membrane with a sealed micropipette (ca. 1 μm radius) controlled with a second micromanipulator.[26] We checked that this method did not cause lethal damage to the examined cells. In fact, its more drastic consequences ought to be less pronounced than those of (nowadays) common biological experiments involving the direct delivery of biochemical or genetic materials into cells' inner compartments through the use of identical micropipettes. The oxidative stress response is presumably stimulated by the instant depolarization of the cell membrane provoked by the rapid interconnection of the two different double layers built up on each face of the cell membrane.

Because of the dendritic electrode surface platinization required to obtain decent electrochemical responses,[26] the ultramicroelectrode capacitances are excessively large, and so are capacitive currents. On the other hand, pricking the cell membrane creates a connection between its cytosol and the extracellular fluid where the electrode is positioned. This induces significant diffusional fluxes of nonelectroactive ions to and from the electrode surface. Thus, double-layer capacitances and therefore capacitive currents are expected to vary significantly following the membrane intrusion. Both features prevent the use of transient methods such as chronoamperometry or even moderately fast cyclic voltammetry (viz., ca. 50–100 V s^{-1}) to investigate the nature of the products released by the cell during oxidative bursts.[33] Slow voltammetric scans (viz., at scan rates of a few volts per second or less) would be compatible since the capacitive currents would be small enough, but they could not be used here because the potential scan durations would then be comparable to the signal half-widths (compare Figure 2a), which would thus alter the observed voltammetric measurements.

Any electrochemical analysis of oxidative bursts requires then a series of independent measurements performed at a set of different constant potentials. Such collections of independent measurements are necessarily obtained from a series of different cells, namely, one cell per potential investigated. This built-in requirement introduces another great difficulty, which is among the largest in any bioelectrochemical investigation involving isolated living cells. Indeed, in essence, cell responses exhibit a strong variability. Thus, the parameters featuring two events recorded for two different cells cannot be directly compared even when performed under identical conditions. Any comparison of responses obtained at different potentials thus requires that a statistically significant population of cells is investigated at each potential so that a statistical analysis may be performed. In our experiments, this necessitated the averaging of 25–40 individual cell responses at a given electrode potential depending on the cell culture

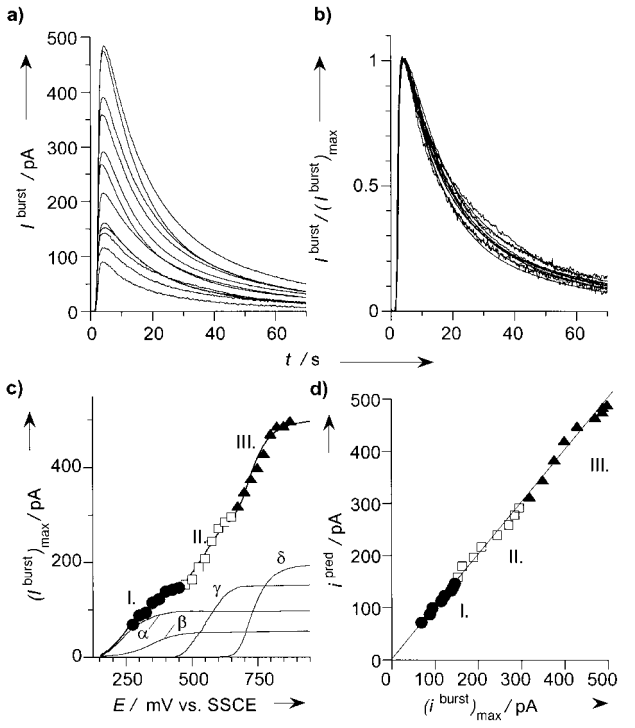

Figure 2. Oxidative cellular bursts monitored in vivo. a) Time dependence of the anodic currents monitored at different potentials after the stimulation of a human fibroblast by the micropipette, when the electrode (10 μm radius) is positioned at $h = 5$ μm above the cell. From bottom to top: the constant electrode potential E was changed from 300 to 850 mV vs. SSCE in steps of 50 mV. Each curve represents the average of 25–40 individual events recorded at each constant potential in order to be statistically significant; b) Normalization of the traces shown in a) relative to their individual maximum current values $(I^{burst})_{max}$; c) Variations of $(I^{burst})_{max}$, the maximum current intensity of the spikes shown in a) as a function of the electrode potential (circles, squares, and triangles; different symbols are used to help to distinguish the three waves I–III; one data point every 25 mV). Solid curves: voltammogram reconstructed (unlabeled curve) by arithmetic addition of the individual steady-state voltammograms (noted α, β, γ, and δ, and shown at the bottom of the same panel) obtained at the same electrodes for (α) H_2O_2 (1.4 μM), (β) ONO_2^- (1.7 μM), (γ) NO (19 μM), and (δ) NO_2^- (4 μM) (see text); d) Correlation (slope 0.99; correlation coefficient = 0.989; 25 data points) between the reconstructed and experimental voltammograms shown by the unlabeled solid curve shown in c) (see text).

examined. Then the standard deviations were small enough for observing reproducible (i.e., culture-to-culture and day-to-day) and meaningful electrochemical data (i.e., with a ±5% precision at 70% confidence, or ±10% at 95% confidence).[34] For example, the set of data shown in Figure 2a represents more than 500 individual experiments. All the data shown hereafter have been obtained through this long, repetitive, but necessary procedure. Since fibroblasts need to be examined in a biologically compatible aerobic environment [air-saturated PBS (phosphate buffer saline) in a Petri dish at 25 °C], they are necessarily surrounded by a large concentration of oxygen (0.24 mM). The presence of the highly reducible oxygen molecule at such a high concentration forbids any investigation of cathodic potential ranges to avoid blasting the cell with significant quantities of superoxide and hydrogen peroxide prior and during the experiments. So, the analytical detection and identification of species released

by the cell have to be performed far from the very foot of the oxygen reduction wave, that is, at potentials larger than 0.275 V versus SSCE (saturated sodium calomel electrode).

Figure 2a shows the significant variations of the oxidative stress amplitude in terms of the corresponding oxidation current, I^{burst}, as a function of the detection potential over the electrochemical window of interest. Interestingly, when each of these current traces is normalized to its current maximum, namely, upon plotting $I^{burst}/(I^{burst})_{max}$ as performed in Figure 2b, they can almost be superimposed, which shows that their time courses are extremely similar. Despite this close current–time behavior, plotting the current maxima, $(I^{burst})_{max}$, as a function of the detection potential (Figure 2c) demonstrates the presence of at least three different electrochemical waves (labeled I to III).

From now on, it is necessary to identify the species leading to each wave by comparing the electrochemical signature of the oxidative stress response to that of each different species which may be involved in the response. Waves II and III are characteristic of $NO^{\bullet}$ (wave II: $E_{1/2} = 0.555 \pm 0.010$ V vs. SSCE; one-electron oxidation) and NO_2^- (wave III: $E_{1/2} = 0.730 \pm 0.010$ V vs. SSCE; two-electron oxidation) oxidations respectively at our electrodes as demonstrated by their perfect matches to the steady-state voltammograms of authentic bulk solutions of these species obtained under identical conditions (PBS solutions) at the same electrodes (compare with the voltammograms labeled γ and δ shown in Figure 2c).

The first oxidation wave (I), with an apparent half-wave potential at 0.290 ± 0.010 V versus SSCE, does not correspond to any expected species (vide supra), and moreover is noticeably more sluggish than waves II and III. Furthermore, based on collection-efficiency measurements as a function of the cell-electrode distance,[29] the diffusion coefficient(s) relative to the species oxidized at this wave is (are) comparable (i.e. ca. 2×10^{-5} cm^2 s^{-1}) to those of NO_2^- or H_2O_2 in the PBS. This demonstrates that the molecule(s) giving rise to wave I is (are) comparable to NO_2^- or H_2O_2 in terms of size (viz., molecular weight) and interactions with the PBS medium. This establishes in particular that wave I cannot feature at all the oxidation of proteins or of larger biological molecules released by the cell through the puncture made in its membrane. Most of all, the time course of the released flux corresponding to this wave is extremely similar to those observed for $NO^{\bullet}$ and NO_2^- (Figure 2b).

All these independent features strongly suggest that the species oxidized at wave I is (are) closely related—molecularly speaking—to H_2O_2 or NO_2^-. This points to the involvement of ONO_2^-, $O_2^{\bullet -}$, or H_2O_2 (vide supra). The involvement of $O_2^{\bullet -}$ per se can be easily ruled out because wave I is by far too anodic. In PBS, authentic samples of H_2O_2 are oxidized almost in the correct potential range ($E_{1/2} = 0.250 \pm 0.005$ V vs. SSCE; two-electron wave) at our platinized carbon electrodes, and yet they give rise to a better-defined and less anodic wave (compare with wave α in Figure 2c). This prompted us to examine and characterize in vitro the ONO_2^- oxidation electrochemical wave in order to be able to assess its possible involvement in the oxidation process(es) detected at wave I.

Voltammetric study of peroxynitrite solutions (in vitro)

Steady-state response (*low scan rates*): The electrochemical behavior of peroxynitrite solutions could not be investigated under physiological conditions (i.e., pH = 7.4 in PBS) since its decomposition kinetics are too fast at this pH ($t_{1/2} \approx 1$ s at $T = 25\,^{\circ}$C)[13] to allow the preparation of stock solutions. Note however, that in vivo, the diffusion time from the cell to the electrode surface is within the millisecond timescale so that if ONO_2^- is produced, less than 10% of the amount released should decompose during the time taken to the electrode surface. However, this does not apply during in vitro experiments because of the necessity to prepare stock solutions. We needed then to define experimental conditions so that bulk solutions of peroxynitrite could be investigated without significant decomposition during the analytical measurement.

The decomposition of peroxynitrite in dilute solution is highly sensitive to pH as a result of the central involvement of its transient protonated form ($pK_a = 6.8$).[13, 14, 35] Therefore, the kinetics could be considerably slowed down by performing the experiments at basic pHs. pHs ≥ 12 could not be used with platinized carbon fiber electrodes, since their surfaces underwent a rapid loss of sensitivity, possibly resulting from their alteration by formation of oxides.[36, 37] In vitro voltammetric experiments were then performed in moderately basic aqueous media, in which the peroxynitrite concentration did not reasonably evolve ($t_{1/2}$ ranging from a few minutes at pH ≈ 9 to one hour at pH ≈ 12). The synthesis of stock solutions of peroxynitrite was achieved by ozonation of slightly alkaline azide solutions, a method which provided concentrated solutions (ranging from 30 to 80 mM) virtually devoid of hydrogen peroxide and of metal complexes, which are both electroactive species that would interfere with the oxidation mechanism and the analysis.[38] Diluted peroxynitrite solutions were subjected to linear sweep voltammetry at low sweep rates ($v < 50$ mV s^{-1} where v is the voltammetric scan rate), which led to steady-state voltammetric responses at our microelectrodes. Under these conditions, two well-defined oxidation waves (labeled O_A and O_B) were observed on platinized carbon fiber microelectrodes at $E_{1/2} = 0.35 \pm 0.02$ V and 0.72 ± 0.01 V versus SSCE, respectively (Figure 3b).

During the reaction time (ca. ≈1 h) required for the synthesis of peroxynitrite, aliquots of the reaction mixture were collected and tested both electrochemically with platinized carbon fiber microelectrodes and spectrophotometrically. The magnitude of the plateau currents of the waves O_A and O_B increased with time (Figure 3b) following for wave O_A a strict correlation with the absorbance of the respective solution measured at $\lambda_{max} = 302$ nm (Figure 3a), which is characteristic of the peroxynitrite anion.[38] The spontaneous decomposition kinetics of peroxynitrite solutions at several pHs were analyzed by both methods. A good correlation between the decay rate constants of wave O_A plateau current and that of the absorbance at 302 nm was again obtained (Figure 3c). Conversely, wave O_B did not significantly change with time after completion of the synthesis. The first-order kinetics rate constants determined from wave O_A decay are close to those reported in the literature for peroxynitrite: that

0947-6539/01/0719-4174 $ 17.50+.50/0 *Chem. Eur. J.* **2001**, *7*, No. 19

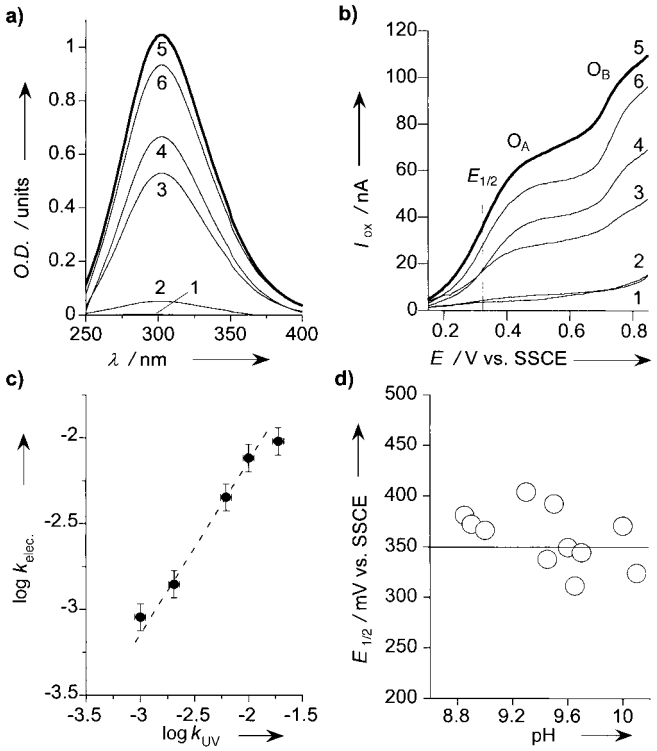

Figure 3. Peroxynitrite production during the ozonation of an azide solution (pH = 12) followed by: a) spectrophotometry ($\lambda_{max} = 302$ nm) or b) steady-state electrochemistry (20 mV s^{-1}). Measurements were taken at 0 (1), 10 (2), 30 (3), 50 (4), 55 (5; bold curves in a,b), and 60 (6) minutes after the beginning of ozonation. Waves O_A and O_B correspond to the oxidation of ONO_2^- and NO_2^-, respectively, at platinized carbon-fiber microelectrodes (10 μm diameter); c) Correlation (five data points representing the average of three different experiments each) between the decomposition rate constants of peroxynitrite solutions followed by UV spectrophotometry (log k_{uv}; cell thermostated at 22 °C) and electrochemistry (log k_{elec}; unthermostated cell, see Experimental Section) at several pH values (from 8.7 up to 10.2 from right to left). A dashed line with unity slope is shown to help the comparison; d) Evidence for the absence of any correlation between $E_{1/2}$ of wave O_A and pH over the range $8.8 < pH < 10.2$. All electrochemical experiments shown in this figure were carried out with platinized carbon fiber microelectrodes (10 μm diameter) in phosphate buffer solutions of ONO_2^-.

is, $k = 8 \times 10^{-5}\ s^{-1}$ (pH = 12), to be compared with $k = 1 \times 10^{-5}\ s^{-1}$ (as calculated at pH = 12 in ref. [35]) or $k = 8 \times 10^{-5}\ s^{-1}$ (pH = 11 in ref. [39]). All these features strongly suggest that the species oxidized at wave O_A is the peroxynitrite anion, while that detected at wave O_B is a side product formed in parallel with ONO_2^- during the in situ synthesis of stock solutions. The latter is presumably NO_2^- in agreement with its known oxidation potential and previous reports.[13, 39, 40] Furthermore, additions of aliquots of concentrated nitrite solutions to the peroxynitrite solution proportionally increased the magnitude of the plateau current of this wave. This came as no surprise, since Pryor et al. had already shown that nitrite ions were produced during the synthesis of ONO_2^- according to the method employed in the present work.[38] Once nitrite ions were formed, they did not undergo any further homogeneous chemical transformations over the timescale of the experiments at the alkaline pH values considered here, in agreement with the fact that the plateau current of wave O_B remained constant.

Figure 3d demonstrates the absence of any correlation between the half-wave potential of wave O_A and the pH over a range confined to basic conditions (see above). $E_{1/2}$ remained around 0.35 ± 0.03 V versus SSCE in the range $8.8 \leq pH \leq 10.2$ despite a significant scatter and poor reproducibility of the data (i.e., within the precision of their determination). This scattering and poor reproducibility are presumably due to uncontrolled alterations of the platinized surfaces of the electrodes in these basic media since, as will be established below, this $E_{1/2}$ value reflects not only the thermodynamics but is strongly controlled by the kinetics of the initial electron transfer. Therefore, it is likely that this value (i.e., within the precision of its determination) strongly depends on the electrode surface properties, which are affected by exposure to basic solutions[36, 37] (note that the platinized electrode surfaces were checked to be stable at neutral pH upon using the H_2O_2 oxidation wave so this poor accuracy could not affect the in vivo results). Because of this accuracy problem, and since it affected only the heterogeneous rate constant of electron transfer, the electrochemical signature for peroxynitrite oxidation at our platinized electrodes was obtained by averaging all the independent steady-state voltammograms (whose $E_{1/2}$ values are represented in Figure 3d) after translating numerically their individual potential scales so that their translated $E_{1/2}$ values all coincided with the average value of 0.35 V versus SSCE established above. This led to the voltammogram labeled β in Figure 2c.

The absence of any systematic dependence of $E_{1/2}$ on the pH indicates that the electrochemical process does not involve protons.[41] This implies that wave O_A represents the direct oxidation of ONO_2^- (viz., not of its conjugate acid, through a CE (chemical-electrochemical reaction sequence),[41] which is consistent with the fact that $pH > pK_a = 6.8$ over the range investigated. Furthermore, since the maximum oxidation degree of nitrogen is +VI as it is in $ONO_2^{\bullet}$,[35] this implies that the primary redox reaction is then necessarily a one-electron process giving rise to $ONO_2^{\bullet}$ as the primary intermediate.

It then follows that the two electrochemical processes at waves O_A and O_B may be represented by the following primary Equations (8) and (9).

$$\text{Wave } O_A\text{: } ONO_2^- - e^- \longrightarrow ONO_2^{\bullet} \longrightarrow \text{etc.} \quad (8)$$

$$\text{Wave } O_B\text{: } NO_2^- + 2OH^- - 2e^- \longrightarrow NO_3^- + H_2O \quad (9)$$

Equation (9) involves the formation of nitrate ions. However, these are not electroactive at our electrodes either in these in vitro experiments or during the in vivo ones. In particular, if nitrate ions were released by the cell during oxidative bursts, this would remain undetected by our method.

Transient voltammetry (*high scan rates*): This series of experiments was aimed at detecting possible short-lived intermediates formed upon the electrochemical oxidation of peroxynitrite and at estimating the kinetic parameters of their reactions. Transient voltammetry was conducted on bare platinum microelectrodes of 125 and 500 μm diameters. They

were used and preferred to platinized carbon-fiber microelectrodes since their capacitance was much smaller, leading to better-defined Faradaic voltammograms at sweep rates higher than 1 V s^{-1}. The two waves O_A and O_B described in the previous section were again observed with these pure platinum microelectrodes. The most anodic of them (wave O_B, data not shown) agreed again with the transient voltammetric oxidation of nitrite into nitrate [Eq. (9)]. Wishing to focus our investigations on the peroxynitrite response (wave O_A), we then limited the voltammetric potential window between -0.2 and 0.8 V versus SSCE in the subsequent studies (Figure 4 a,b), therefore obviating any eventual interference

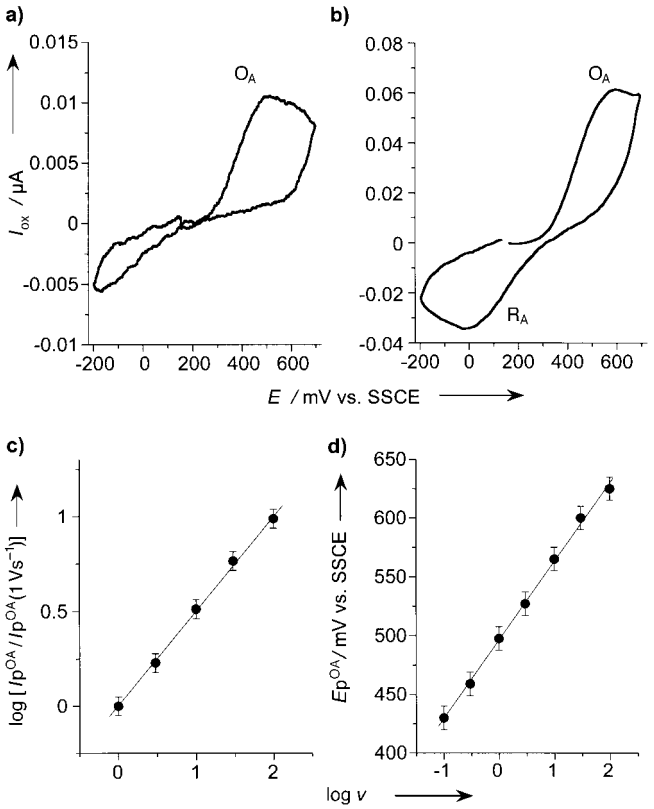

Figure 4. Transient cyclic voltammetry of ONO_2^- (12 mM) oxidation in vitro (phosphate solutions, pH = 10.5) at platinum disk microelectrodes [125 µm diameter in a), b); 125 to 500 µm diameters in c), d)]. a), b) Transient voltammograms recorded at 1 (a) or 30 (b) V s^{-1}; c) Variations of the peak current intensity (I_p^{OA}) with the scan rate (slope 0.5, correlation coefficient = 0.998, five data points representing the average of three different experiments each); d) Variations of the peak potential (E_p^{OA}) with the scan rate (slope 0.067 V, correlation coefficient = 0.998, seven points, three experiments for each point).

due to oxygen at more cathodic potentials and excluding the nitrite wave O_B and its oxidation products from the voltammetric window. However, in some experiments, the potential window corresponding to the oxygen reduction range was voluntarily explored voltammetrically to ascertain that O_2 was not produced within our voltammetric timescales as a follow-up product of ONO_2^- oxidation (vide infra).[13]

Peroxynitrite oxidation experiences a diffusional control as revealed by the 1/2 slope value of the log(I_{pa}) versus log v plot (i.e., $I_{pa} \propto v^{1/2}$,[41] Figure 4c). The slope of the E_{pa} vs. log v variations was close to 67 mV (Figure 4d), an expected feature for overall kinetics controlled by the initial electron-transfer kinetics ($\alpha_{ox} = 0.45$).[41] Figure 4a and 4b show transient cyclic voltammograms obtained with peroxynitrite solutions at 1 and 30 V s^{-1}, respectively. In the former case, no reverse step was detected in the potential window of interest, while in the latter a well-defined reduction wave R_A was observed upon scan reversal. Clearly, the species giving rise to the reduction wave R_A was formed during the oxidation process at wave O_A, but underwent further chemical transformations so that its reduction could no longer be detected at smaller scan rates. Its lifetime was approximately 0.1 s judging from the onset of its wave when scanning at 10 V s^{-1}. To investigate some elements relating to the nature of the species detected at the reduction wave R_A associated with the oxidation wave O_A, the following experiments were performed: i) the scan rate was set at 100 V s^{-1} so that the reduction wave R_A was fully developed; ii) the potential scan was continuously cycled between a fixed value ($E_{an} = 0.7$ V vs. SSCE) located on the plateau of wave O_A and a variable more cathodic potential (E_{cath}). When E_{cath} was too anodic to encompass wave R_A, the current intensity of wave O_A dropped rapidly during the first few repetitive scans, and this showed that ONO_2^- could not be regenerated in the diffusion layer under these conditions. Conversely, when E_{cath} was set at a more negative value so as to encompass increasing fractions of wave R_A, the decay of wave O_A with the number of repetitive scans was slower. When E_{cath} reached the diffusion limit of wave R_A, the system of waves O_A/R_A remained steady upon continuous cycling. This behavior is characteristic and demonstrates that the reduction of the species observed at wave R_A regenerates quantitatively the peroxynitrite ion within the diffusion layer. This and the fact that the half-sum of the peak potentials of waves O_A and R_A is independent of the scan rate, of the pH, and of the peroxynitrite concentration, points out that the tandem of electrochemical waves O_A/R_A represents the slow charge-transfer process in Equation (10).

$$ONO_2^- - e^- \rightleftharpoons ONO_2^{\bullet} \quad (10)$$

Simulations of these voltammograms allowed the determination of the following characteristics of the peroxynitrite electrochemical oxidation: $E^0 = 0.27 \pm 0.02$ V versus SSCE for the couple $ONO_2^{\bullet}/ONO_2^-$; transfer coefficient, $\alpha_{ox} = 0.45$; heterogeneous rate constant, $k_{ox}^{el} = 10^{-3}$ cm s^{-1}. These values are consistent with the plots in Figure 4c, d, as well as with control of the wave by the kinetics of the heterogeneous electron transfer [Eq. (10)] under steady-state conditions (see above). The existence of the nitrosyldioxyl radical, $ONO_2^{\bullet}$, was postulated to account for the previous observation of an identified intermediate during the reaction of $NO^{\bullet}$ with O_2 in the gaseous phase,[42] although it has been suggested more recently that the detected species was a $NO^{\bullet}/O_2$ adduct and not $ONO_2^{\bullet}$.[43] In aqueous solutions, $ONO_2^{\bullet}$ has been considered as an intermediate in the autoxidation mechanism of $NO^{\bullet}$.[44] Finally, a formal reduction potential has been calculated for the couple $ONO_2^{\bullet}/ONO_2^-$ on the basis of thermodynamic considerations by Koppenol et al., namely, $E^0 = 0.43 \pm 0.13$ V versus a normal hydrogen electrode (NHE)

0947-6539/01/0719-4176 $ 17.50+.50/0 *Chem. Eur. J.* **2001**, *7*, No. 19

(i.e., $E^0 = 0.19 \pm 0.13$ V vs. SSCE).[35] This predicted range encompasses reasonably well the value determined in the present work, $E^0 = 0.27 \pm 0.02$ V versus SSCE [Eq. (10)].

Follow-up kinetics of $ONO_2^{\bullet}$: Bearing in mind that the radical $ONO_2^{\bullet}$, unless quickly re-oxidized, spontaneously decomposes so that wave R_A is not observable, we can therefore best explain the whole process at wave O_A by an EC electrochemical scheme.[41] The follow-up chemical step may be a first-order (or pseudo first-order) process [Eq. (11)] or a second-order homogeneous reaction as suggested previously [Eq. (12)].[13]

$$ONO_2^{\bullet} \longrightarrow \text{etc.} \quad (11)$$

$$2\,ONO_2^{\bullet} \longrightarrow \text{etc.} \quad (12)$$

Occurrence of the reactions in Equations (11) or (12) can be distinguished based upon the dependence of the current peak intensity of wave R_A at a given scan rate on the concentration of the substrate. Indeed, upon increasing the concentration, the current peak intensity of wave R_A relative to that of wave O_A should remain constant for a first-order reaction [Eq. (11)].[41] Conversely, it should decrease in relative value for second-order kinetics [Eq. (12)].[41] Experimentally, the current ratio was found to be independent of the concentration (tested from 6 to 20 mM) so that a second-order reaction such as that in Equation (12) is definitely ruled out.

Therefore, the most plausible sequence of events is represented by Equation (10) at higher sweep rates ($v \geq 10$ V s^{-1}), or Equations (10) and (11) at lower sweep rates ($v \leq 1$ V s^{-1}). The mechanisms postulated in the literature for the decomposition of $ONO_2^{\bullet}$ include an overall decay to O_2 and $NO^{\bullet}$, thought to occur either directly or via a short-lived dimer intermediate.[13] The direct path may be excluded, since the reduction wave of O_2 was not observed (note that in vitro experiments were conducted in deaerated solutions, so formation of O_2 within voltammetric times would have been detected if this was produced upon oxidation of peroxynitrite). This clearly establishes that the first-order decay of wave R_A ($t_{1/2} \approx 0.1$ s) does not correspond at all to a direct decomposition of $ONO_2^{\bullet}$ into O_2 and $NO^{\bullet}$. It cannot yield its previously postulated dimer on the way to O_2 and $NO^{\bullet}$ formation either since this would correspond to a second-order process. Therefore, Equation (11), which takes place within the short voltammetric timescale may only be rationalized upon considering a different first-order decay, presumably involving an isomerization of the primary radical $ONO_2^{\bullet}$ formed, according to Equation (13).

$$ONO_2^{\bullet} \longrightarrow [ONO_2^{\bullet}]^* \quad (13)$$

This isomerized species may then well dimerize, as suggested previously for $ONO_2^{\bullet}$,[13] to eventually decay, yielding O_2 and NO_2 at markedly longer times than available with voltammetric investigations [Eq. (14)].

$$2\,ONO_2^{\bullet} \rightarrow 2[ONO_2^{\bullet}]^* \rightarrow [(ONO_2^{\bullet})_2]^* \longrightarrow O_2 + 2\,NO_2 \quad (14)$$

Such a mechanism would indeed respect the observed first-order kinetics for $ONO_2^{\bullet}$ decay, while affording a second-order rate for the ultimate production of O_2 and NO_2 as postulated previously.[13]

To conclude this section, we wish to discuss several possible structures for the isomerized species noted as $[ONO_2^{\bullet}]^*$ in Equations (13) and (14). Since ONO_2^- exists as two isomeric forms, *cis* and *trans* [Eq. (15)], the most stable being the *cis* form, one may then tentatively propose that the isomerization in Equation (13) features a similar *cis–trans* process occurring at the level of the radical.

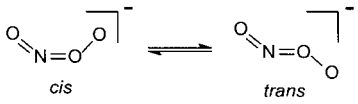

(15)

However, this appears extremely unlikely on the basis of the previously reported quantum chemical investigation.[45] A third isomer ought then to be considered, for example, the tentative structure shown in [Eq. (16)], which does not appear unreasonable considering those disclosed in ref. [35].

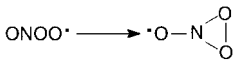

(16)

Relevance to cellular oxidative bursts: We established above the electrochemical characteristics of a molecule of great biological interest, the peroxynitrite ion ONO_2^-. We have shown that ONO_2^- can be oxidized at the surface of platinized carbon fiber or bare platinum microelectrodes. An experimental value of $E^0 = 0.27 \pm 0.02$ V versus SSCE could be derived from fast-scan cyclic voltammograms of the $ONO_2^{\bullet}/ONO_2^-$ redox couple. It was also established that ONO_2^- oxidation follows an EC mechanism, in which the electrochemical process is the rate-limiting step. The follow-up chemical reaction involving $ONO_2^{\bullet}$ was found to be a first-order process presumably leading to the isomerization of the initially formed radical with $t_{1/2} \approx 0.1$ s.

Our goal in undertaking this study of ONO_2^- electrochemical oxidation was to characterize the steady-state voltammograms of peroxynitrite solutions on platinized carbon fiber microelectrodes so as to compare them to the waves recorded in vivo during cell experiments. Peroxynitrite samples are oxidized in the potential range of wave I (Figure 2c) giving a slightly more anodic wave (wave β in Figure 2c: $E_{1/2} = 0.350 \pm 0.020$ V vs. SSCE, 1-electron wave; vs. $E_{1/2} = 0.290$ V vs. SSCE for wave I). Conversely, H_2O_2 samples give rise to a slightly less anodic wave (wave labeled α in Figure 2c, $E_{1/2} = 0.250 \pm 0.005$ V vs. SSCE, 2-electron wave). Such close oxidation waves, that is, with half-wave potentials located on each side of wave I strongly suggest that the slowly developing oxidation wave detected for cells may not be a single wave at all but may actually result from the accidental convolution of those of H_2O_2 and ONO_2^-. To test this hypothesis, we examined therefore if the in vivo oxidation current, I^{burst}, observed at wave I (i.e., between 0.275 and 0.475 V vs. SSCE; Figure 2c, solid circles) could be described as a linear combination of the oxidation currents I_α and I_β measured in vitro for authentic solutions of H_2O_2 and ONO_2^-

in PBS at the same electrodes. Thus, the experimental in vivo oxidation current was arbitrarily decomposed as in Equation (17).

$$I^{burst} = f \times [\varepsilon \times I_{\alpha} + (1-\varepsilon) \times I_{\beta}] \quad (17)$$

In the above equation, f is a scaling factor, and ε a weighting factor. The factors f and ε do not have the same effect on the wave, and they are independent parameters. Indeed, ε affects the shape of the "reconstructed" wave, while f only scales its intensity. Since I_{β} and $(I_{\alpha} - I_{\beta})$ have known values at each potential as deduced from the in vitro experiments, ε was readily obtained through a linear correlation procedure by rewriting Equation (17) as Equation (18).

$$I^{burst} \propto [I_{\beta} + \varepsilon \times (I_{\alpha} - I_{\beta})] \quad (18)$$

This procedure afforded $\varepsilon = 0.45$ (slope 2.10, correlation coefficient 0.994, nine data points) for the conditions shown in Figure 2c; $f = 2.1$ was then obtained at once from the slope of the ensuing linear correlation. This treatment led to an experimentally "reconstructed" voltammogram (unlabeled solid line in Figure 2c) based on a mixture of H_2O_2 and ONO_2^- and of $NO^{\bullet}$ and NO_2^- as determined above. This "reconstructed" voltammogram neatly agreed with the experimental set of waves I–III recorded during oxidative bursts, as attested also by the excellent correlation in Figure 2d (slope 0.99; correlation coefficient = 0.989; 25 data points).

Conclusion

The direct, unmediated electrochemical signature of peroxynitrite, ONO_2^-, an important biologically active species resulting from the near diffusion-limited reaction between $NO^{\bullet}$ and $O_2^{\bullet -}$, is reported for the first time. This species is oxidized at platinum surfaces to the peroxynitryl radical, $ONO_2^{\bullet}$, which can either be reduced back to peroxynitrite (at scan rates larger than $10\ V\ s^{-1}$), or decay by a first-order process with an EC mechanism to product(s) still to be characterized (at scan rates smaller than $1\ V\ s^{-1}$). The electrochemical parameters ($E^0 = 0.27$ V vs. SSCE, $\alpha_{ox} = 0.45$, $k_{ox}^{el} = 10^{-3}\ cm\ s^{-1}$) have been determined, as well as an estimate ($t_{1/2} \approx 0.1$ s) for the lifetime of the electrogenerated $ONO_2^{\bullet}$ radical in PBS.

This allowed, for the first time, the direct characterization of ONO_2^- in the oxidative burst emitted by human fibroblasts upon mechanical stimulation, together with H_2O_2, $NO^{\bullet}$, and NO_2^-. This was achieved by the deconvolution of the amperometric responses obtained by application of the semiartificial synapse method based on microelectrodes. Such results, especially taking into account the rather short duration of the activation time (less than a tenth of a second), appear extremely important owing to the likely involvement of peroxynitrite in several human pathological conditions. The fast production, detected within less than a tenth of a second, of ONO_2^- by living cells submitted to an oxidative stress implies therefore the rapid action of pre-assembled enzymatic systems. Owing to the rapid formation of peroxynitrite by coupling of $NO^{\bullet}$ and $O_2^{\bullet -}$, it is acceptable to assume that NO-synthase and NADPH-oxidase, two enzymes responsible for the synthesis of $NO^{\bullet}$ and $O_2^{\bullet -}$, are simultaneously triggered immediately after the rapid cell membrane depolarization.

Experimental Section

Single cell experiments: All the experiments have been performed at 25 °C in Petri dishes placed on the stage of an inverted microscope. The electrode and micropipette were positioned with respect to the cell with two micromanipulators. All the details, including those concerning the platinized carbon fiber microelectrodes construction, electrochemical apparatus, PBS solutions, or cell culture, and handling have been reported previously.[26] The fibroblasts used in this study came from a control human cell line (198VI) established from a skin biopsy and were kindly provided by Dr. A. Sarasin (UPR CNRS 2169, Villejuif, France). Cells were grown in MEM F12 medium (Gibco BRL) with fetal calf serum (10%) in an incubator (5% CO_2, 37 °C). Confluent monolayers of fibroblasts were harvested by trypsination. From 1000 to 2000 cells were then re-suspended in Petri dishes (3.5 cm diameter, Costar 3035) and stored in the incubator for 48 h during which they spontaneously adhered to the Petri dish bottom. Cells were then washed three times in PBS buffer before experiments, which were only performed with isolated cells to avoid biochemical interference between them through local diffusion of products released during oxidative bursts.

In Vitro Voltammetric experiments: All reagents except peroxynitrite and nitric oxide were purchased from Sigma. Aqueous solutions were prepared with water obtained from a Millipore Milli-Q system. The in vitro test experiments were carried out in deaerated PBS (phosphate buffer saline, 10 mM Na_2HPO_4/NaH_2PO_4, 137 mM NaCl, and 2.7 mM KCl) containing either $NaNO_2$ (10 mM), ONO_2^- (6 to 20 mM), H_2O_2 (1 mM), or $NO^{\bullet}$ (2 mM saturated solutions). In the latter case, $NO^{\bullet}$ (l'Air Liquide, 99.99%) was passed through NaOH (4 M) in order to scavenge any NO_x impurities and bubbled (with great caution under a fumehood) through thoroughly deaerated PBS buffer. Peroxynitrite was synthesized by ozonation of slightly alkaline azide solutions according to the procedure developed by Pryor et al.[38] Briefly, ozone was generated by passing oxygen through an ozonator (Welsbach) undergoing a silent electrical discharge (120 V). The gas stream from the ozonator, containing ≈1% O_3 in oxygen, was continuously bubbled through a glass-frit in an aqueous solution of sodium azide (100 mL, 0.1–0.2 M) and NaOH (10 mM), chilled at 0 °C in an ice bath. Unreacted ozone was trapped in a solution of potassium iodide (10%) in water. The peroxynitrite concentration was spectrophotometrically monitored ($\varepsilon = 1.670\ M^{-1}\ cm^{-1}$ at $\lambda_{max} = 302$ nm; Beckman DU-7400) by collecting aliquots (1 mL) of the reaction mixture at intervals of 5 to 10 min, and after dilution (8 to 12-fold) in NaOH (10 mM). The ozonation was stopped once the absorption maximum was detected (reached after 55 minutes in Figure 3a,b; in a general case usually between 40 to 80 minutes, depending on the ozonation conditions and the initial concentration of azide). Indeed, continuing ozonation after this point would have resulted in a progressive scavenging of peroxynitrite to form nitrite. This method led to peroxynitrite solutions containing just traces of azide (<3‰) and devoid of H_2O_2.[38] Stock solutions of peroxynitrite (concentrations ranging from 30 to 80 mM) were frozen and stored at −20 °C and used within 2 weeks, a period during which they did not decompose. During the experiments, the defrosted solutions were kept at 0 °C in an ice bath to minimize the spontaneous peroxynitrite decay.

Bare platinum and platinized carbon-fiber microelectrodes were used for the electrochemical measurements.[26, 33] Platinum disk electrodes were made from cross-sectioned glass-encased platinum wires (10, 125, or 500 μm diameter, Goodfellow), which were polished with fine sand papers (P1200 and P4000, Presi, France) and diamond paste (1 μm, Presi) before use.[46] Platinized carbon-fiber microelectrodes were fabricated as previously described.[26] In the present experiments (in vitro and in vivo), the electrodeposition of platinum on the carbon microelectrodes was limited at a maximum charge of 90 μC. All potentials referred to a saturated sodium chloride calomel electrode SSCE (Tacussel-Radiometer, France; E vs.

0947-6539/01/0719-4178 $ 17.50+.50/0 *Chem. Eur. J.* **2001**, *7*, No. 19

SSCE = E vs. SCE + 5 mV, 25 °C) unless otherwise indicated, since the conventional SCE reference electrode could not be used in biological systems as a result of possible alteration of cellular activity by potassium ion leakage. In vitro voltammetric experiments were performed at 25 °C in a conventional three-electrode electrochemical cell equipped with a homemade potentiostat with electronic ohmic drop compensation.[47] Amperometric experiments (E = +0.5 V vs. SSCE) used in the study of the peroxynitrite decomposition rate (Figure 3c) were carried out in a miniaturized cell constructed within an Eppendorf tip (500 µL). This allowed very quick mixing (just a few seconds) of the stock solution of peroxynitrite at pH = 12 with the buffer at a desired pH and allowed us to work under similar conditions to those for the spectrophotometric analysis (however, this miniaturized cell could not be thermostated; since the UV cell was thermostated at 22 °C, this may well explain why the correlation in Figure 3c has the correct slope of unity but not a zero intercept). Digital voltammetric simulations were carried out using Digisim 2.1 (Bioanalytical Systems Inc., West Lafayette, USA).

The UV detection of the peroxynitrite decomposition was carried out with the cell thermostated at 22 °C. Owing to the biological relevance of peroxynitrite, biologically compatible buffers such as PBS, TRIS [Trizma base, Tris(hydroxymethyl)aminomethane, 0.1M], and CAPS [3-(cyclohexylamino)-1-propanesulfonic acid, 0.1M] were chosen according to their useful pH range (PBS: 7–8; TRIS: 7–9; CAPS: 9.7–11.1) and used in the electrochemical and spectrophotometric studies. Some experiments were carried out in phosphate solutions at pH > 9.5, which were prepared from the PBS buffer by adjusting the pH with concentrated NaOH.

Acknowledgements

This work was supported in part by CNRS (UMR 8640 "PASTEUR"), Ecole Normale Supérieure, and the French Ministry of Research (MENESR). P.d.O. thanks CNRS for a research fellowship. D.B. and M.E. thank MENESR for their PhD grants. Dr. A. Sarasin (UPR CNRS 2169, Villejuif, France) is cordially thanked for providing the fibroblasts cultures used in this study.

[1] B. Halliwell, J. M. C. Gutteridge, *Free Radicals in Biology and Medicine*, 3rd ed., Oxford University Press, Oxford, **1999**.
[2] H. Sies, *Angew. Chem.* **1986**, *98*, 1061; *Angew. Chem. Int. Ed. Engl.* **1986**, *25*, 1058.
[3] K. J. A. Davies, F. Ursini, *The Oxygen Paradox*, CLEUP University Press, Padova, **1995**.
[4] B. Chance, *Annu. Rev. Biophys. Bio.* Palo Alto, **1991**.
[5] B. Chance, G. R. William, *J. Biol. Chem.* **1955**, *230*, 409.
[6] H. Sies, *Metabolic Compartimentation*, Academic Press, New York, **1982**.
[7] A. W. Segal, O. T. G. Jones, *Nature* **1978**, *276*, 515.
[8] B. Meier, A. Jesaitis, A. Emmendorffer, J. Roesler, M. T. Quinn, *Biochem. J.* **1993**, *289*, 481.
[9] B. Meier, A. R. Cross, J. T. Hancock, F. J. Kaup, O. T. Jones, *Biochem. J.* **1991**, *275*, 241.
[10] C. von Sonntag, *The Chemical Basis of Radiation Biology*, Taylor & Francis, London, **1987**.
[11] R. Hattori, K. Sase, H. Eizawa, K. Kosuga, T. Aoyama, R. Inoue, S. Sasayama, C. Kawai, Y. Yui, K. Miyahara, *Int. J. Cardiol.* **1994**, *47*, S71.
[12] R. Wang, A. Ghahary, Y. J. Shen, P. G. Scott, E. E. Tredget, *J. Invest. Dermatol.* **1996**, *106*, 419.
[13] R. Kissner, T. Nauser, P. Bugnon, P. Lye, W. H. Koppenol, *Chem. Res. Toxicol.* **1997**, *10*, 1285.
[14] H. Ischiropoulos, J. Beckman, J. Crow, J. Royall, N. Kooy, *Methods Enzymol.* **1995**, *7*, 109.
[15] R. Radi, *Chem. Res. Toxicol.* **1998**, *11*, 720.
[16] R. Meli, T. Nauser, W. H. Koppenol, *Helv. Chim. Acta* **1999**, *82*, 722.
[17] G. L. Squadrito, W. A. Pryor, *Free Radical Bio. Med.* **1998**, *25*, 392.
[18] D. Salvemini, M. P. Jensen, D. P. Riley, T. P. Misko, *Drug News & Perspect.* **1998**, *11*, 204.
[19] J. T. Groves, *Curr. Opin. Chem. Biol.* **1999**, *3*, 226.
[20] A. Lachgar, N. Sojic, S. Arbault, D. Bruce, A. Sarasin, C. Amatore, B. Bizzini, D. Zagury, M. Vuillaume, *J. Virol.* **1999**, *73*, 1447.
[21] J. Beckman, T. Beckman, J. Chen, P. Marshall, B. Freeman, *Proc. Natl. Acad. Sci. USA* **1990**, *87*, 1620.
[22] J. Kanski, T. Koppal, D. A. Butterfield, *Anal. Lett.* **1999**, *32*, 1183.
[23] A. Denicola, J. M. Souza, R. Radi, *Proc. Natl. Acad. Sci. USA* **1998**, *95*, 3566.
[24] M. Kelm, R. Dahmann, D. Wink, M. Feelisch, *J. Biol. Chem.* **1997**, *272*, 9922.
[25] J. Xue, X. Ying, J. Chen, Y. Xian, L. Jin, *Anal. Chem.* **2000**, *72*, 5313.
[26] S. Arbault, P. Pantano, J. A. Jankowski, M. Vuillaume, C. Amatore, *Anal. Chem.* **1995**, *67*, 3382.
[27] T. J. Schroeder, J. A. Jankowski, K. T. Kawagoe, R. M. Wightman, C. Lefrou, C. Amatore, *Anal. Chem.* **1992**, *64*, 3077.
[28] C. Amatore, Y. Bouret, L. Midrier, *Chem. Eur. J.* **1999**, *5*, 2151.
[29] C. Amatore, S. Arbault, D. Bruce, P. de Oliveira, M. Erard, M. Vuillaume, *Faraday Discuss.* **2000**, *116*, 319.
[30] C. Amatore, S. Arbault, D. Bruce, P. de Oliveira, M. Erard, N. Sojic, M. Vuillaume, *Analusis* **2000**, *28*, 506.
[31] S. Arbault, P. Pantano, N. Sojic, C. Amatore, M. Best-Belpomme, A. Sarasin, M. Vuillaume, *Carcinogenesis* **1997**, *18*, 569.
[32] K. T. Kawagoe, J. A. Jankowski, R. M. Wightman, *Anal. Chem.* **1991**, *63*, 1589.
[33] S. Arbault, PhD thesis, Université Denis Diderot (Paris VII, France), **1996**.
[34] D. Bruce, PhD thesis, Université Pierre et Marie Curie (Paris VI, France), **2000**.
[35] W. H. Koppenol, J. J. Moreno, W. A. Pryor, H. Ischiropoulos, J. S. Beckman, *Chem. Res. Toxicol.* **1992**, *5*, 834.
[36] S. B. Hall, E. A. Khudaish, A. L. Hart, *Electrochim. Acta* **1998**, *43*, 579.
[37] S. B. Hall, E. A. Khudaish, A. L. Hart, *Electrochim. Acta* **1998**, *43*, 2015.
[38] W. A. Pryor, R. Cueto, X. Jin, W. H. Koppenol, M. Ngu-Schwemlein, G. L. Squadrito, P. L. Uppu, R. M. Uppu, *Free Radical Biol. Med.* **1995**, *18*, 75.
[39] S. Pfeiffer, A. C. F. Gorren, K. Schimdt, E. R. Werner, B. Hansert, D. S. Bohle, B. Mayer, *J. Biol. Chem.* **1997**, *272*, 3465.
[40] W. H. Koppenol, *Free Radical Bio. Med.* **1998**, *25*, 385.
[41] A. Bard, L. Faulkner, *Electrochemical Methods. Fundamentals and Applications*, New York, **1980**.
[42] S. Bhatia, J. H. Hall, *J. Phys. Chem.* **1980**, *84*, 3255.
[43] M. L. McKee, *J. Am. Chem. Soc.* **1995**, *117*, 1629.
[44] S. C. Goldstein, J. Lind, G. Merenyi, *Chem. Res. Toxicol.* **1999**, *12*, 132.
[45] H.-H. Tsai, T. P. Hamilton, J.-H. M. Tsai, M. van der Woerd, J. G. Harrison, M. J. Jablonsky, J. S. Beckman, W. H. Koppenol, *J. Phys. Chem.* **1996**, *100*, 15087.
[46] C. Amatore, L. Thouin, M. F. Bento, *J. Electroanal. Chem.* **1999**, *463*, 45.
[47] C. Amatore, C. Lefrou, F. Pflüger, *J. Electroanal. Chem.* **1989**, *270*, 43.

Received: March 7, 2001 [F3114]